Journal of Luminescence 214 (2019) 116598

Contents lists available at ScienceDirect

Journal of Luminescence

journal homepage: www.elsevier.com/locate/jlumin

Plasmon-enhanced upconversion and quantum-cutting of water-soluble $Au@SiO_2/NaYF_4:Tb^{3+},Yb^{3+}@NaYF_4$ nanocomposites

Lin Lin[a,b,c,1], Zhipeng Yu[a,1], Zhezhe Wang[a,b,c], Zhuohong Feng[a,b,c], Feng Huang[a,b,c], Lili Huang[a], Qionghua Dai[a], Fengfen Zhang[d], Zhiqiang Zheng[a,b,c,*]

[a] College of Physics and Energy, Fujian Normal University, Fuzhou 350117, China
[b] Fujian Provincial Key Laboratory of Quantum Manipulation and New Energy Materials, Fuzhou 350117, China
[c] Fujian Provincial Collaborative Innovation Center for Optoelectronic Semiconductors and Efficient Devices, Xiamen 361005, China
[d] Fujian Provincial Key Laboratory of Advanced Materials Oriented Chemical Engineering, Fuzhou 350117, China

ARTICLE INFO

Keywords:
Quantum-cutting
Upconversion
Rare-earth ions
Localized surface plasmon resonance
Gold nanorods

ABSTRACT

$Au@SiO_2/NaYF_4:Tb^{3+},Yb^{3+}@NaYF_4$ nanocomposites are acquired by combining $Au@SiO_2$ nanorods with ligand-free $NaYF_4:Tb^{3+},Yb^{3+}@NaYF_4$ nano-particles in water solution due to the electrostatic attraction. Plasmon-enhanced upconversion (UC) and quantum-cutting (QC) are both obtained and optimized in these nanocomposites by adjusting SiO_2 shell thickness and concentrations of $Au@SiO_2$. While the thickness of SiO_2 shell is 35 nm, the enhancement factor of UC and QC reaches maximum as 1.91 and 3.47 times, respectively. The nanocomposites may be applied in biological fluorescence label, super-resolution imaging and solar cells, etc.

1. Introduction

Upconversion (UC) and quantum-cutting (QC) are two well-known special luminescence phenomena. UC converts one high-energy photon to multiple low-energy photons. QC is the inverse process of UC. Both of UC and QC can be applied to many fields with wide overlap, such as bio-imaging (UC [1,2] & QC [3]), super-resolution imaging (UC [4,5]), temperature sensor (UC [6]), mercury free fluorescent lamps (QC [7]), displays (UC [8] & QC [9,10]) and solar cells (UC [11] & QC [12]). Thus, the ion pairs providing both UC and QC have more broad prospects, e.g. utilizing both of ultraviolet and near-infrared photons for solar cells [13]. Among these ion pairs, Tb^{3+}-Yb^{3+} ion pairs have special UC and QC mechanism (UC: cooperative sensitization UC [14–16], QC: cooperative energy transfer [17–19]). Therefore, they exhibit strong UC and QC luminescence even if the concentration of Tb^{3+} is high [12,14,18]. Moreover, the luminescence of Tb^{3+}-Yb^{3+} is less susceptible to surface quenching effect [14].

However, the applications of UC and QC are limited by low quantum efficiency. To solve this problem, noble metal nano-particles (NPs) are utilized to enhance the luminescence of rare-earth ions via localized surface plasmon resonance (LSPR). Great progress has been made in research on plasmon-enhanced UC [20–25]. On the contrary, since plasmon-enhanced QC was firstly reported by our group [17], only a few papers have been published about this topic. Comparatively speaking, obtaining both of plasmon-enhanced UC and QC in water solution of nanocomposites is more valuable in specific applications (e.g. bio-imaging), and more uncommon because nanocomposites dispersed in solution are usually unstable and easy to be separated [26].

Specifically, the plasmon-enhancement effect is greatly influenced by the spacing distance between the noble metal NP and the rare-earth ion [26–28]. Only when the distance is appropriate (generally tens of nanometers), great enhancement can be detected [27–31]. When the distance is too far away, the rare-earth ion will be out of range of enhanced electric field. While the distance is too close, energy transfer from the rare-earth ion to the noble metal NP will occur, leading to luminescence quenching. Therefore, it is important to confirm the optimal spacing distance.

In this paper, $Au@SiO_2$ nanorods (NRs) and ligand-free $NaYF_4:Tb^{3+},Yb^{3+}@NaYF_4$ NPs were combined to form water-soluble nanocomposites, denoted as $Au@SiO_2/NaYF_4:Tb^{3+},Yb^{3+}@NaYF_4$. In the nanocomposites, Au NRs with extinction peak of 980 nm were applied to enhance both UC and QC of Tb^{3+}-Yb^{3+} ion pairs, equipped with SiO_2 shell to adjust the spacing distance. Plasmon-enhanced UC and QC were both detected in water solution of the nanocomposites with optimal spacing distance, which was reported for the first time in our knowledge.

* Corresponding author. College of Physics and Energy, Fujian Normal University, Fuzhou 350117, China.
E-mail address: zqzheng@fjnu.edu.cn (Z. Zheng).
[1] The first two authors contribute equally to this work.

https://doi.org/10.1016/j.jlumin.2019.116598
Received 24 April 2019; Received in revised form 1 July 2019; Accepted 2 July 2019
Available online 02 July 2019

2. Experimental

Chemical reagents and instruments. Oleic acid (90%), $TbCl_3{\cdot}6H_2O$ (99.99%) and $YbCl_3{\cdot}6H_2O$ (99.9%) were purchased from Alfa Aesar. 1-octadecene (90%), $YCl_3{\cdot}6H_2O$ (99.9%), $NaBH_4$ and ascorbic acid (AA) were purchased from Sigma Aldrich. HCl (1 mol L^{-1}) were purchased from Scharlab. $AgNO_3$ were purchased from Aladdin. Sodium Oleate (NaOL) was purchased from TCI. Tetraethoxysilane (TEOS), ethanol, methanol, cyclohexane, $HAuCl_4{\cdot}4H_2O$, cetyltrimethylammonium bromide (CTAB), HCl (37 wt%) and NaOH were purchased from Sinopharm Chemical Reagent Co. Ltd. All the reagents unspecified purity were analytical pure grade.

The SEM (scanning electron microscope) and TEM (transmission electron microscope) images were taken on the Hitachi SU-8010 SEM and JEM-2100 TEM, respectively. The X-ray diffraction (XRD) patterns were measured on the Rigaku MiniFlex II X-ray diffractometer under Cu K_α radiation (λ = 0.154056 nm). The extinction spectra were taken on PerkinElmer Lambda 950 UV-Vis-NIR spectrophotometer. The fluorescence spectra and luminescence decay curves were obtained from Horiba Jobin Yvon Fluorolog 3–22 spectrophotometer equipped with dual Xe lamps (450 W) and a 980 nm laser (4 W) for light source, a R928P photomultiplier and an InGaAs infrared detector for signal detection. The zeta potentials were carried out on a Zetasizer Nano-ZSE zeta potential analyzer (Malvern). All the measurements were taken at room temperature.

Synthesis of ligand-free $NaYF_4$:Tb^{3+},Yb^{3+}@$NaYF_4$ NPs. First, $YCl_3{\cdot}6H_2O$, $TbCl_3{\cdot}6H_2O$ and $YbCl_3{\cdot}6H_2O$ (1 mmol in total) were dissolved in oleic acid and 1-octadecene, and heated for dehydration. The concentrations of Tb^{3+} and Yb^{3+} were 15% and 10%, respectively, which were confirmed as optimal concentrations in our previous reports [32]. Methanol solution of NaOH and NH_4F were added. Then, the solution was heated rapidly to 300 °C. The oleate-capped $NaYF_4$:Tb^{3+},Yb^{3+} NPs were collected via centrifugation and dispersed in 5 ml cyclohexane [26]. Secondly, oleate-capped $NaYF_4$:Tb^{3+},Yb^{3+} NPs were dispersed in the solution of $YCl_3{\cdot}6H_2O$ (1 mmol) in oleic acid and 1-octadecene. Then the process above was repeated with only $YCl_3{\cdot}6H_2O$ (1 mmol) as starting materials to obtain oleate-capped $NaYF_4$:Tb^{3+},Yb^{3+}@$NaYF_4$ NPs. Third, a proper amount of HCl was added into as-prepared oleate-capped $NaYF_4$:Tb^{3+},Yb^{3+}@$NaYF_4$ NPs solution under high-speed stirring to remove oleate ligand. The ligand-free $NaYF_4$:Tb^{3+},Yb^{3+}@$NaYF_4$ NPs were collected from extracted lower water layer via high-speed centrifugation and redispersed in 4 ml deionized water.

Synthesis of Au@SiO_2 NRs. The Au NRs were prepared following Ref. [33]. 5 ml $HAuCl_4$ solution (0.5 mM) and 5 ml CTAB solution (0.2 M) were mixed (solvent unspecified was deionized water, the same below). Afterwards, 0.6 ml fresh $NaBH_4$ solution (0.01 M) was added to the mixture with vigorous shaking to form seed solution. Besides, 7.0 g CTAB and 1.234 g NaOL were dissolved in 250 ml warm deionized water. Then, 24 ml $AgNO_3$ solution (4 mM), 250 ml $HAuCl_4$ (1 mM) and 4.2 ml HCl (37 wt%) were added successively. 1.25 ml AA (0.064 M) and 0.4 ml seed solution was added successively with high-speed stirring. The Au NRs were formed over 12 h at room temperature. Finally, the solution was centrifuged, washed and re-dispersed in 40 ml deionized water.

Afterwards, 8 ml deionized water, 100 µl CTAB (0.1 M) and 100 µl NaOH (0.1 M) were added into 2 ml as-prepared Au NR solution. Then, the solution was heated to 45 °C with the addition of TEOS solution in ethanol (10 vol%) for coating. Finally, the Au@SiO_2 NRs was centrifuged, washed and re-dispersed in 15 ml ethanol. The SiO_2 shell thickness can be adjusted by the addition amount of TEOS solution (30 µl - 160 µl).

3. Results and discussion

The $NaYF_4$: Tb^{3+}, Yb^{3+} NPs are all hexagonal β-$NaYF_4$ phase (No. 16–0334), according to the XRD patterns (Fig. 1). Based on the SEM images (Fig. 2), oleate-capped $NaYF_4$: Tb^{3+}, Yb^{3+} NPs are ball-like with a diameter of 14 nm. The oleate-capped $NaYF_4$: Tb^{3+}, Yb^{3+}@ $NaYF_4$ NPs are rod-like with a length of 23 nm and a diameter of 18 nm. After the removal of oleate ligands, the ligand-free $NaYF_4$: Tb^{3+}, Yb^{3+}@ $NaYF_4$ NPs are shortened and turn to ball-like with a diameter of 17 nm. The results infer that the inert $NaYF_4$ shell still exists after the removal of oleate, beneficial to the luminescence of $NaYF_4$ NPs, because the inert shell can reduce surface quenching processes and enhance the luminescence effectively [34,35]. Furthermore, the ligand-free NPs can be well dispersed to water for further preparation.

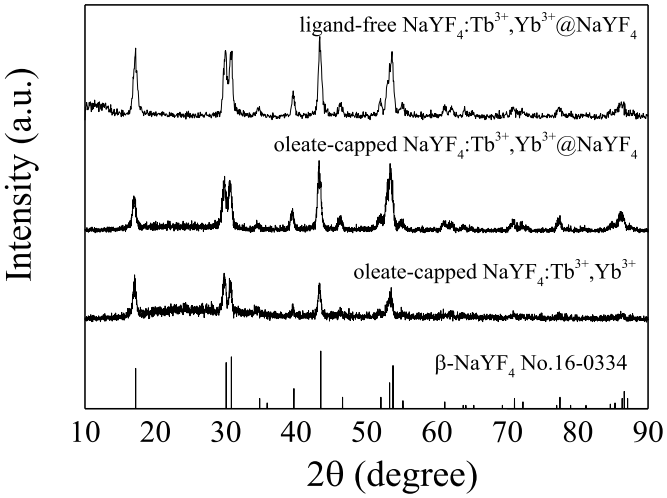

Fig. 1. XRD patterns of $NaYF_4$: Tb^{3+}, Yb^{3+} and $NaYF_4$: Tb^{3+}, Yb^{3+}@$NaYF_4$ NPs.

For the combination of nanocomposites, Au@SiO_2 NRs with different SiO_2 shell thickness (15 nm - 45 nm) were prepared. The SEM images and the extinction spectra of Au NRs and Au@SiO_2 NRs (Fig. 3) show that the SiO_2 shell are uniform (Fig. 3a–e), and the extinction peak is shifted to long wavelength with increasing SiO_2 shell thickness due to the change of dielectric constant around Au NRs after coating (Fig. 3f).

The zeta potentials of Au@SiO_2 NRs and $NaYF_4$:Tb^{3+},Yb^{3+}@$NaYF_4$ NPs are calculated from zeta potential distribution (Fig. 4a) as +30.3 mV and −14.1 mV, respectively. The results infer that the $NaYF_4$:Tb^{3+},Yb^{3+}@$NaYF_4$ NPs can be adsorbed on the surface of Au@ SiO_2 NRs in water solution to form Au@SiO_2/$NaYF_4$:Tb^{3+},Yb^{3+}@ $NaYF_4$ nanocomposites due to the electrostatic attraction [36], which is confirmed by the SEM image of nanocomposites (Fig. 4b). Furthermore, the removal of oleate is described as: $RE(OA) \overset{HCl}{\rightarrow} [REO^-] + H_3O^+ + H(OA)$ [37], where RE and OA is the rare-earth ions and oleate on the surface of $NaYF_4$ NPs, respectively. Thus, on the surface of ligand-free $NaYF_4$ NPs, there is no ligand which can bond to OH group attracted on SiO_2 shell [38,39]. Therefore, the interaction between Au@SiO_2 and $NaYF_4$:Tb^{3+},Yb^{3+}@$NaYF_4$ NPs is not ionic interaction but electrostatic attraction. The nanocomposites can be well dispersed in water, which helps them apply to bio-imaging.

The LSPR peak of Au@SiO_2 in the nanocomposites is represented besides the absorption peaks of Tb^{3+} and Yb^{3+} in the extinction spectra of nanocomposites (inset of Fig. 4b), compared with that of $NaYF_4$:Tb^{3+},Yb^{3+}@$NaYF_4$ NPs. Our aim is obtaining optimal plasmon-enhanced UC and QC both in water solution of these nanocomposites. As mentioned in the introduction, the enhancement strongly depends on the distance between Au NR and RE ions, which is adjusted by varying the SiO_2 shell thickness in the nanocomposites.

Several peaks can be observed in the UC emission spectra of nanocomposites (Fig. 5a–e). The emission peaks located at 486 nm, 543 nm, 584 nm and 620 nm can be attributed to $^5D_4 \rightarrow {}^7F_j$ transitions (j = 6, 5,

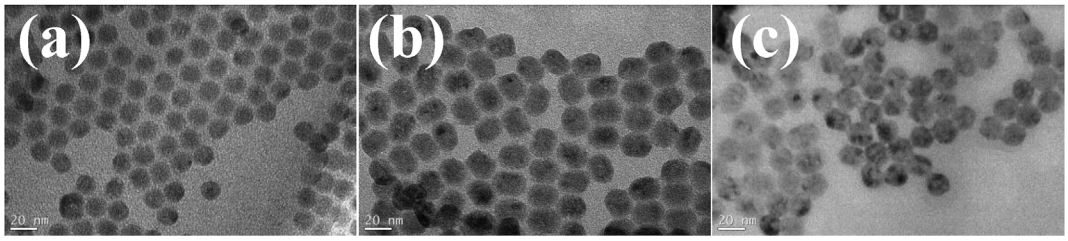

Fig. 2. TEM images of (a) oleate-capped $NaYF_4$: Tb^{3+}, Yb^{3+} NPs; (b) oleate-capped $NaYF_4$: Tb^{3+}, Yb^{3+}@$NaYF_4$ NPs; (c) ligand-free $NaYF_4$: Tb^{3+}, Yb^{3+}@ $NaYF_4$ NPs.

4, 3) of Tb^{3+}, respectively. With each SiO_2 shell thickness, the emission intensity increases then decreases with increasing concentration of $Au@SiO_2$ (this concentration is the molar ratio between Au and $NaYF_4$:Tb^{3+},Yb^{3+}). The increasing is ascribed to LSPR of $Au@SiO_2$. The decreasing is originated from strong extinction of $Au@SiO_2$ on excitation light, which offset the enhancement of LSPR [32]. The enhancement factor (EF) of UC intensity varies with SiO_2 shell thickness and concentrations of $Au@SiO_2$, reaching maximum as 1.91 times

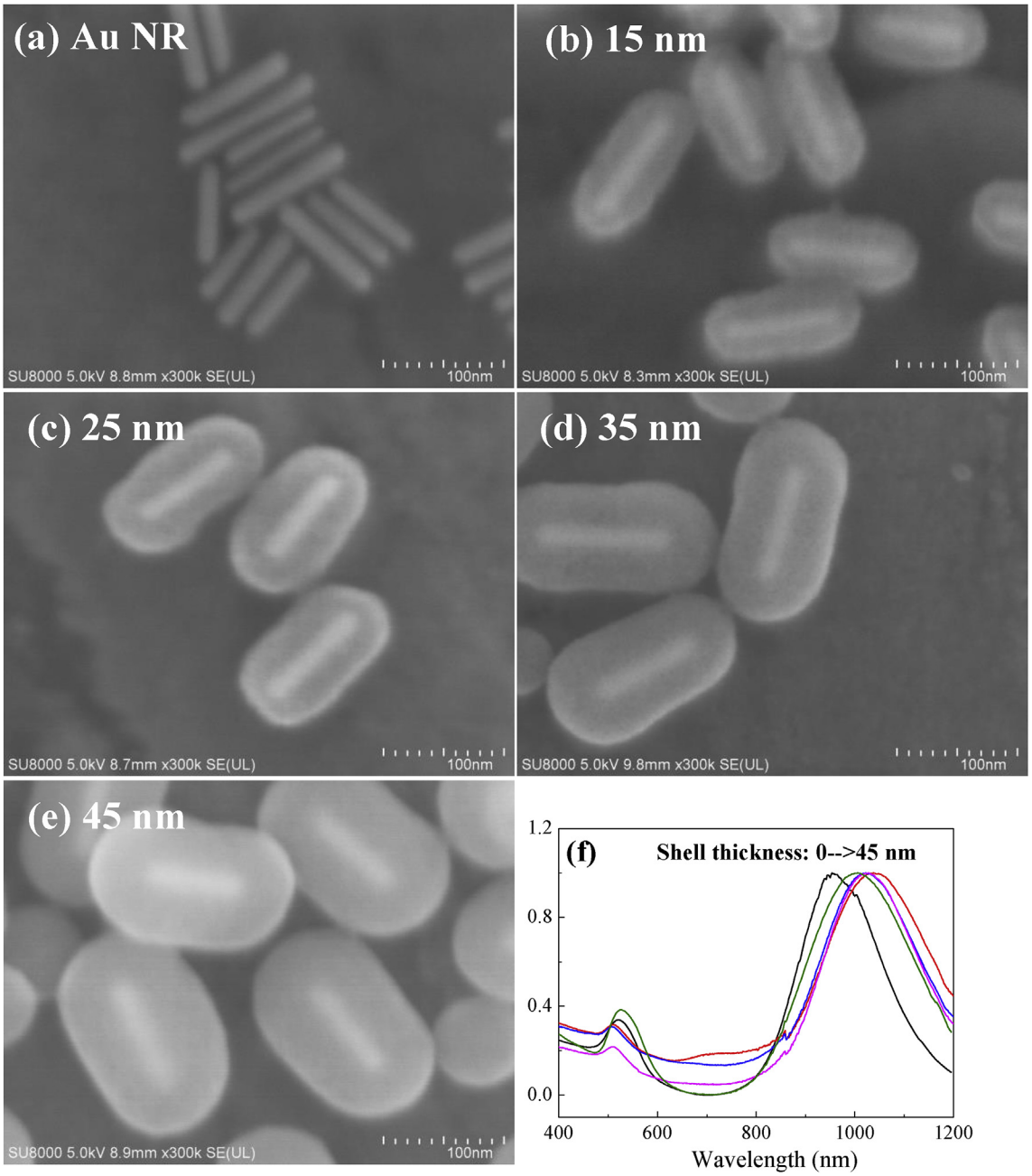

Fig. 3. (a–e) SEM images of Au NRs and $Au@SiO_2$ NRs with different SiO_2 shell thickness; (f) Extinction spectra of corresponding Au NRs and $Au@SiO_2$ NRs.

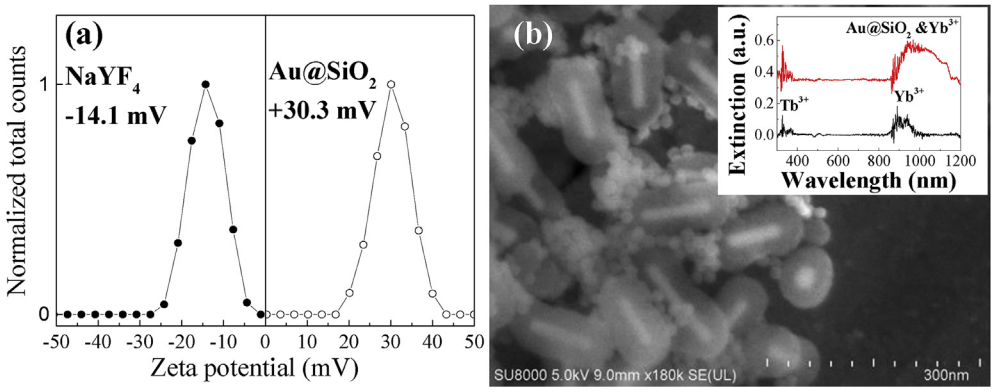

Fig. 4. (a) Normalized zeta potential distribution of water solutions of $Au@SiO_2$ and $NaYF_4$:Tb^{3+},Yb^{3+}@$NaYF_4$; (b) SEM image of $Au@SiO_2$/$NaYF_4$:Tb^{3+},Yb^{3+}@$NaYF_4$ nanocomposites (Inset: Extinction spectra of water solutions of $NaYF_4$: Tb^{3+}, Yb^{3+}@$NaYF_4$ NPs (black) and $Au@SiO_2$/$NaYF_4$: Tb^{3+}, Yb^{3+}@$NaYF_4$ nanocomposites (red)). (For interpretation of the references to colour in this figure legend, the reader is referred to the Web version of this article.)

while the SiO_2 shell thickness is 35 nm. All of the above is depicted in Fig. 5f. It is noticeable that, even if the SiO_2 shell is absent, weak enhancement still can be detected unlike our previous report [26], because the inert $NaYF_4$ shell separates rare-earth ions from Au NRs.

The QC emission spectra of the nanocomposites are depicted in Fig. 6. The excitation wavelength (372 nm) is according to the transition of $^7F_6 \rightarrow {}^5D_3$ of Tb^{3+}, which is the strongest excitation wavelength as we reported before [17,18]. Only one broad band can be observed in each emission spectrum, which is attributed to the transition of $^2F_{5/2} \rightarrow {}^2F_{7/2}$ of Yb^{3+}. The trend of emission intensity with SiO_2 shell thickness and concentrations of $Au@SiO_2$ is similar to the case of UC because of the same reason. EF reaches maximum as 3.47 times, while the SiO_2 shell thickness is 35 nm, the same as that of UC. In addition, the emission band of Yb^{3+} shows shape deformation with increasing concentrations of $Au@SiO_2$. The reason is as follows: General speaking, the maximal enhancement can be obtained while the emission wavelength is the same as the wavelength of LSPR peak of noble metals. Otherwise, the enhancement will be reduced [27]. Since the location of the LSPR

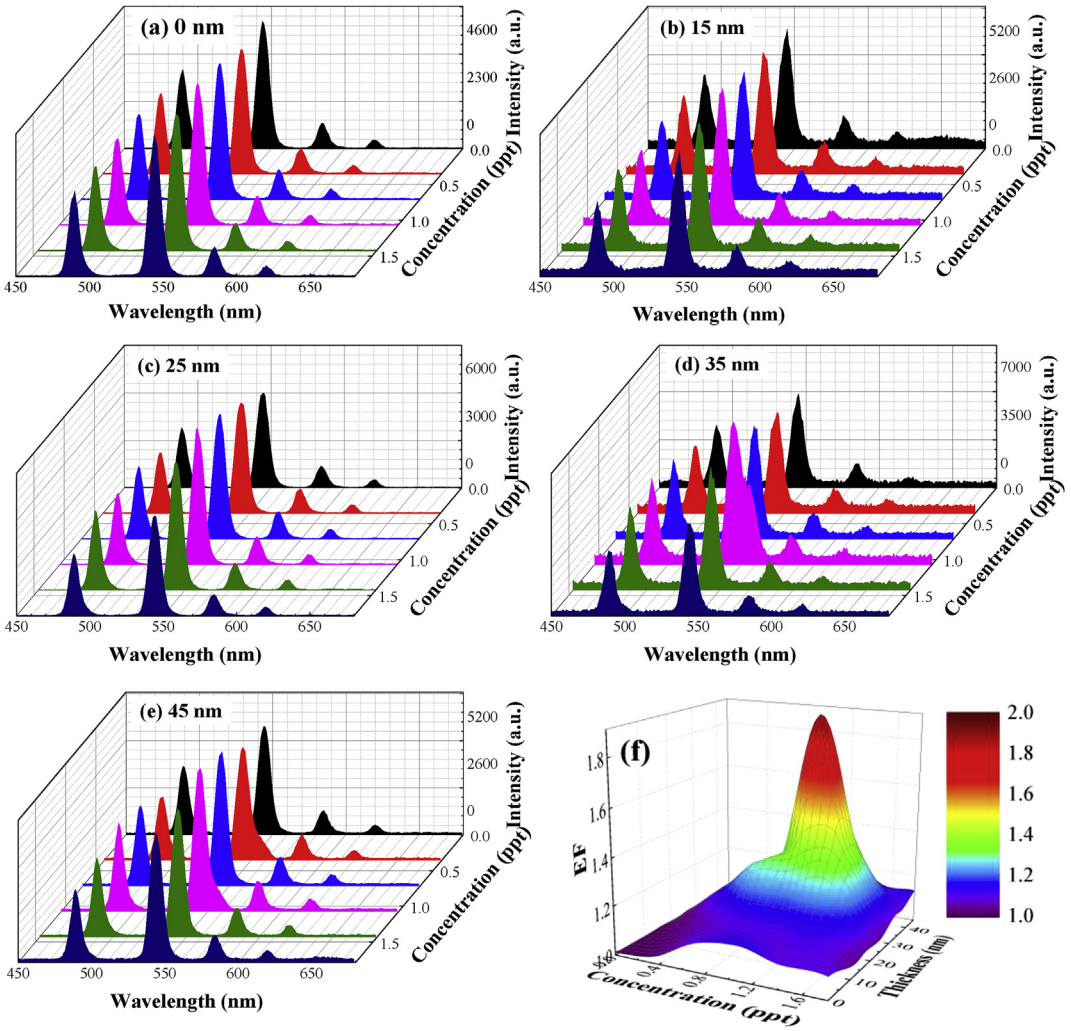

Fig. 5. (a–e) UC emission spectra (λ_{ex} = 980 nm) of $Au@SiO_2$/$NaYF_4$:Tb^{3+},Yb^{3+}@$NaYF_4$ nanocomposites with different SiO_2 shell thickness. (f) Enhancement factor (EF) of UC emission intensity of $Au@SiO_2$/$NaYF_4$: Yb^{3+}, Tb^{3+}@$NaYF_4$ nanocomposites with different SiO_2 shell thickness and concentrations of $Au@SiO_2$

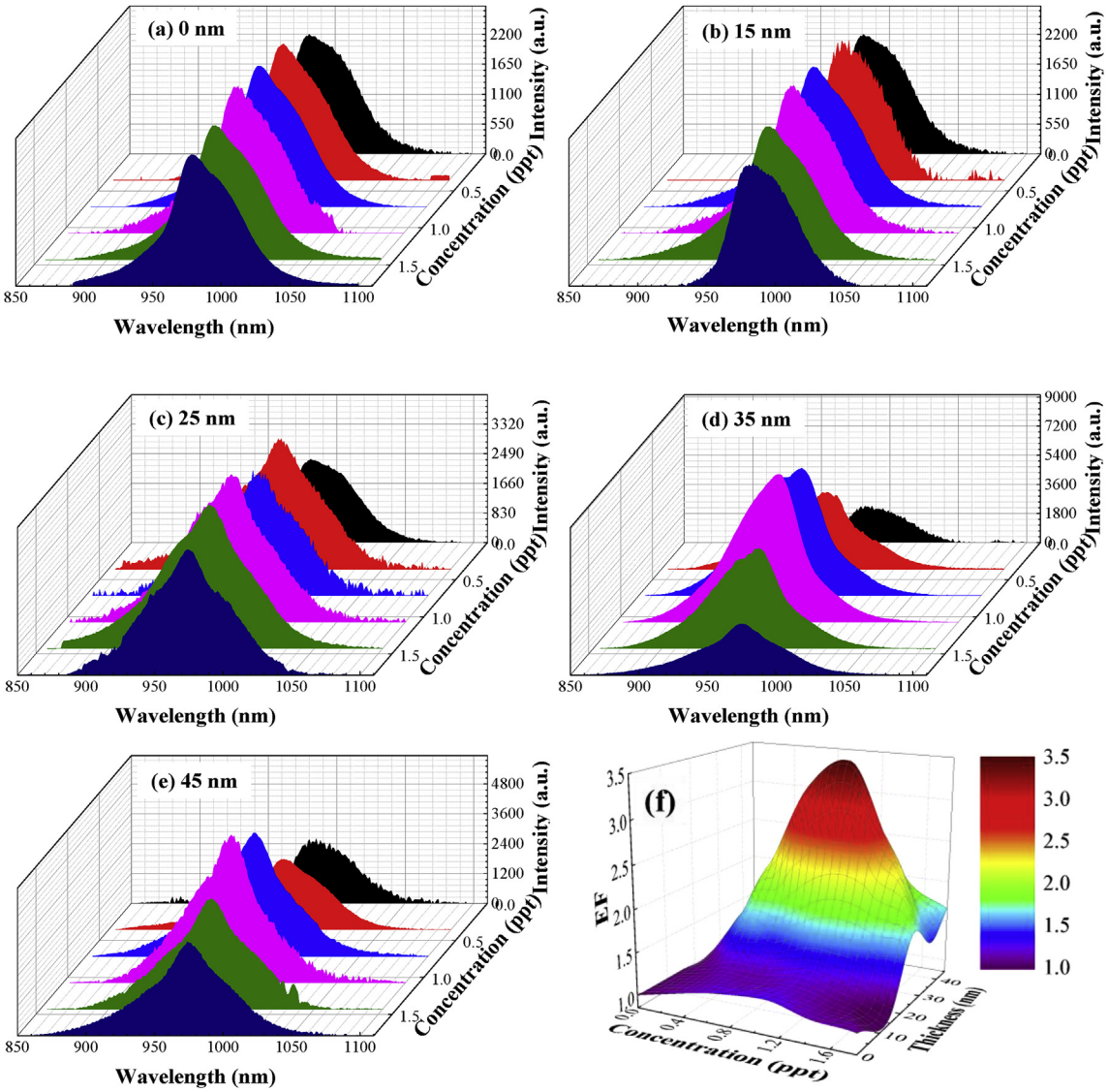

Fig. 6. (a–e) QC emission spectra (λ_{ex} = 372 nm) of Au@SiO_2/$NaYF_4$: Tb^{3+}, Yb^{3+} @$NaYF_4$ nanocomposites with different SiO_2 shell thickness. (f) Enhancement Factor (EF) of QC emission intensity of Au@SiO_2/$NaYF_4$:Tb^{3+}, Yb^{3+}@$NaYF_4$ nanocomposites with different SiO_2 shell thickness.

peak of Au NRs is not completely consistent with that of the emission band of Yb^{3+}, the shape of enhanced emission band is varied [40]. The results also indicate the existence of LSPR peak of Au@SiO_2 in the nanocomposites.

Discussing the differences between the enhancement of UC and QC is interesting. The enhancement mechanism of UC is "absorption matching", because the extinction peak of Au NR is close to the excitation wavelength [26,41,42]. In this case, the enhanced electric field enhances the excitation rate from ground state, leading to the enhancement of emission intensity. On the other hand, the enhancement of QC is originated from "emission matching", since the extinction peak of Au NR is near the emission wavelength [26,41,42]. In this mechanism, the enhanced electric field enhances the radiative transition rate. Thus, the quantum efficiency and the emission intensity are enhanced. In our case, EF of QC is higher than that of UC. The possible reason is: In the case of "emission matching", EF can be written as: $EF = \frac{Q}{Q_0}$ [43], where Q and Q_0 are the quantum efficiency of samples with/without enhancement, respectively. Q and Q_0 can be described as: $Q_0 = \frac{A_r}{A_r + A_{nr}}$ and $Q = \frac{A_r'}{A_r' + A_{nr}}$, where A_{nr} is the non-radiative transition rates of Yb^{3+}, A_r and A_r' are the unenhanced/enhanced radiative transition rates, respectively. Since the non-radiative transition rate of Yb^{3+} is high with high Yb^{3+} concentration [44], the enhancement of radiative transition rate leads to high EF [26]. Based on the luminescence decay curves of the nanocomposites in QC case (Fig. 7), the lifetime of Yb^{3+} emission shortens with increasing concentrations of Au@SiO_2, which proves the radiative transition rate of Yb^{3+} is enhanced by Au@SiO_2. On the contrary, the lifetime of Tb^{3+} emission does not show a clear change, which implies Au@SiO_2 does not influence the radiative transition rate of Tb^{3+} or the energy transfer rate from Tb^{3+} to Yb^{3+}. In addition, although the 4f-4f transitions of rare earth ions contain magnetic dipole transitions besides common electric dipole transitions, the magnetic dipole transitions are roughly 10^5 times weaker than electric dipole transitions in general [45]. Hence, the magnetic dipole transitions and the effect of magnetic field to intensity can be ignored in our cases [46].

4. Conclusions

In this work, Au@SiO_2/$NaYF_4$:Tb^{3+},Yb^{3+}@$NaYF_4$ nanocomposites are successfully prepared from Au@SiO_2 nanorods (NRs) and ligand-free $NaYF_4$:Tb^{3+},Yb^{3+}@$NaYF_4$ NPs. In the water solution of these nanocomposites, plasmon enhanced UC and QC are both obtained via "absorption matching" and "emission matching", respectively. While

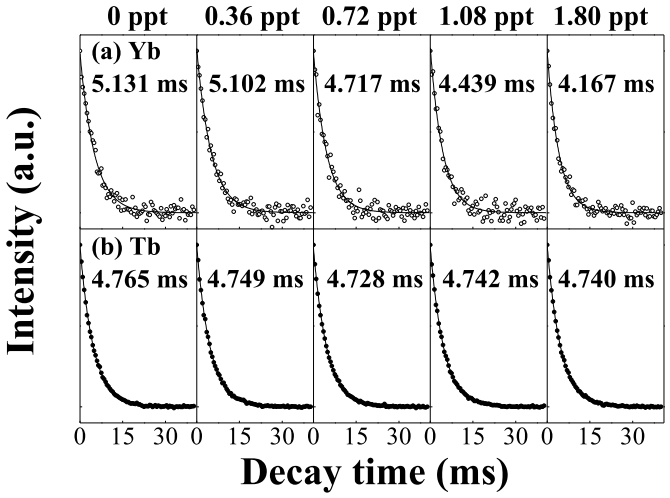

Fig. 7. Normalized luminescence decay curves and corresponding lifetime of $Au@SiO_2/NaYF_4$: Tb^{3+},$Yb^{3+}@NaYF_4$ nanocomposites with different concentrations of $Au@SiO_2$ while SiO_2 shell thickness is 35 nm: (a) Yb^{3+} emission (λ_{ex} = 372 nm, λ_{em} = 980 nm); (b) Tb^{3+} emission (λ_{ex} = 372 nm, λ_{em} = 543 nm).

the SiO_2 shell thickness is 35 nm, the enhancement factor of UC and QC reaches maximum as 1.91 and 3.47 times, respectively. The nanocomposites can be applied in bio-imaging, super-resolution imaging and solar cells, etc.

Conflicts of interest

The authors declare no competing interests.

Acknowledgements

This work was supported by National Natural Science Foundation of China (No. 11204039 and 51202033); Natural Science Foundation of Fujian Province of China (No. 2015J01243, 2016J01213, 2017J01399 and 2019J01283).

References

[1] X.L. Wu, L.G. Xu, W. Ma, L.Q. Liu, H. Kuang, N.A. Kotov, C.L. Xu, Propeller-like nanorod-upconversion nanoparticle assemblies with intense chiroptical activity and luminescence enhancement in aqueous phase, Adv. Mater. 28 (2016) 5907–5915.
[2] R. An, P.P. Lei, P. Zhang, X. Xu, J. Feng, H.J. Zhang, Near-infrared optical and X-ray computed tomography dual-modal imaging probe based on novel lanthanide-doped $K_{0.3}Bi_{0.7}F_{2.4}$ upconversion nanoparticles, Nanoscale 10 (2018) 1394–1402.
[3] T. Yu, D.C. Yu, H.H. Lin, Q.Y. Zhang, Single-band near-infrared quantum cutting of Ho^{3+}-Yb^{3+} codoped KLu_2F_7 phosphors by energy clustering, J. Alloy. Compd. 695 (2017) 1154–1159.
[4] X.W. Cheng, Y. Pan, Z. Yuan, X.W. Wang, W.H. Su, L.S. Yin, X.J. Xie, L. Huang, Er^{3+} sensitized photon upconversion nanocrystals, Adv. Funct. Mater. 28 (2018) 1800208.
[5] Y.J. Liu, Y.Q. Lu, X.S. Yang, X.L. Zheng, S.H. Wen, F. Wang, X. Vidal, J.B. Zhao, D.M. Liu, Z.G. Zhou, C.S. Ma, J.J. Zhou, J.A. Piper, P. Xi, D.Y. Jin, Amplified stimulated emission in upconversion nanoparticles for super-resolution nanoscopy, Nature 543 (2017) 229–233.
[6] P. Cortelletti, A. Skripka, C. Facciotti, M. Pedroni, G. Caputo, N. Pinna, M. Quintanilla, A. Benayas, F. Vetrone, A. Speghini, Tuning the sensitivity of lanthanide-activated NIR nanothermometers in the biological windows, Nanoscale 10 (2018) 2568–2576.
[7] S.R. Jaiswal, N.S. Sawala, P.A. Nagpure, V.B. Bhatkar, S.K. Omanwar, Visible quantum cutting in Tb^{3+} doped $BaGdF_5$ phosphor for plasma display panel, J. Mater. Sci-mater. Electron. 28 (2017) 2407–2414.
[8] Z. Chen, W.R. Wang, S.L. Kang, W.T. Cui, H. Zhang, G.L. Yu, T. Wang, G.P. Dong, C. Jiang, S.F. Zhou, J.R. Qiu, Tailorable upconversion white light emission from Pr^{3+} single-doped glass ceramics via simultaneous dual-lasers excitation, Adv. Opt. Mater. 6 (2018) 1700787.
[9] Y.F. Liu, J.X. Zhang, C.H. Zhang, J. Jiang, H.C. Jiang, High efficiency green phosphor $Ba_9Lu_2Si_6O_{24}$:Tb^{3+}: visible quantum cutting via cross-relaxation energy transfers, J. Phys. Chem. C 120 (2016) 2362–2370.
[10] M.H. Yuan, H.H. Fan, H. Li, S. Lan, S.L. Tie, Z.M. Yang, Controlling the two-photon-induced photon cascade emission in a Gd^{3+}/Tb^{3+}-codoped glass for multicolor display, Sci. Rep. 6 (2016) 21091.
[11] S.M. Lee, P. Dhar, H.D. Chen, A. Montenegro, L. Liaw, D.S. Kang, B.J. Ga, A.V. Benderskii, J.S. Yoon, Synergistically enhanced performance of ultrathin nanostructured silicon solar cells embedded in plasmonically assisted, multispectral luminescent waveguides, ACS Nano 11 (2017) 4077–4085.
[12] W. Shao, C.K. Lim, Q. Li, M.T. Swihart, P.N. Prasad, Dramatic enhancement of quantum cutting in lanthanide-doped nanocrystals photosensitized with an aggregation-induced enhanced emission dye, Nano Lett. 18 (2018) 4922–4926.
[13] W. Shao, G.Y. Chen, T.Y. Ohulchanskyy, C.H. Yang, H. Agren, P.N. Prasad, A core-multiple shell nanostructure enabling concurrent upconversion and quantum cutting for photon management, Nanoscale 9 (2017) 1934–1941.
[14] Q.L. Zou, P. Huang, W. Zheng, W.W. You, R.F. Li, D.T. Tu, J. Xu, X.Y. Chen, Cooperative and non-cooperative sensitization upconversion in lanthanide-doped $LiYbF_4$ nanoparticles, Nanoscale 9 (2017) 6521–6528.
[15] P. Singh, P.K. Shahi, S.K. Singh, S.B. Rai, Photoluminescence, upconversion and quantum-cutting emission in Tm/Tb/Pr and Yb co-doped oxide phosphor: a comparative study, J. Alloy. Compd. 681 (2016) 477–485.
[16] I.A.A. Terra, L.J. Borrero-González, L.A.O. Nunes, M.P. Belançon, J.H. Rohling, M.L. Baesso, O.L. Malta, Analysis of energy transfer processes in Yb^{3+}-Tb^{3+} co-doped, low-silica calcium aluminosilicate glasses, J. Appl. Phys. 110 (2011) 083108.
[17] B. Zheng, S.Y. Xu, L. Lin, Z.Z. Wang, Z.H. Feng, Z.Q. Zheng, Plasmon enhanced near-infrared quantum cutting of KYF_4: Tb^{3+}, Yb^{3+} doped with Ag nanoparticles, Opt. Lett. 40 (2015) 2630–2633.
[18] L. Lin, H. Lin, Z.Z. Wang, J.X. Chen, R.J. Huang, X. Rao, Z.H. Feng, Z.Q. Zheng, Quantum-cutting of KYF_4:Tb^{3+},Yb^{3+} under multiple excitations with high Tb^{3+} concentration, Opt. Mater. 36 (2014) 1065–1069.
[19] L.D.A. Florencio, L.A. Gomez-Malagon, B.C. Lima, A.S.L. Gomes, J.A.M. Garcia, L.R.P. Kassab, Efficiency enhancement in solar cells using photon down-conversion in Tb/Yb-doped tellurite glass, Sol. Energy Mater. Sol. Cell. 157 (2016) 468–475.
[20] D.Y. Li, D.L. Zhou, W. Xu, X. Chen, G.C. Pan, X.Y. Zhou, N. Ding, H.W. Song, Plasmonic photonic crystals induced two-order fluorescence enhancement of blue perovskite nanocrystals and its application for high-performance flexible ultraviolet photodetectors, Adv. Funct. Mater. 28 (2018) 1804429.
[21] W. Xu, X. Chen, H.W. Song, Upconversion manipulation by local electromagnetic field, Nano Today 17 (2017) 54–78.
[22] W. Xu, T.K. Lee, B.S. Moon, H.W. Song, X. Chen, B. Chun, Y.J. Kim, S.K. Kwak, P. Chen, D.H. Kim, Broadband plasmonic antenna enhanced upconversion and its application in flexible fingerprint identification, Adv. Opt. Mater. 6 (2018) 1701119.
[23] W. Xu, S. Xu, Y.S. Zhu, T. Liu, X. Bai, B. Dong, L. Xu, H.W. Song, Ultra-broad plasma resonance enhanced multicolor emissions in an assembled Ag/$NaYF_4$:Yb,Er nanofilm, Nanoscale 4 (2012) 6971–6973.
[24] Z. Yin, H. Li, W. Xu, S.B. Cui, D.L. Zhou, X. Chen, Y.S. Zhu, G.S. Qin, H.W. Song, Local field modulation induced three-order upconversion enhancement: combining surface plasmon effect and photonic crystal effect, Adv. Mater. 28 (2016) 2518–2525.
[25] D.L. Zhou, D.L. Liu, W. Xu, Z. Yin, X. Chen, P.W. Zhou, S.B. Cui, Z.G. Chen, H.W. Song, Observation of considerable upconversion enhancement induced by $Cu_{2-x}S$ plasmon nanoparticles, ACS Nano 10 (2016) 5169–5179.
[26] L. Lin, Z.P. Yu, Z.Z. Wang, B. Zheng, Z.H. Feng, Z.Q. Zheng, Plasmon-enhanced luminescence of $Ag@SiO_2$/β-$NaYF_4$:Tb^{3+} nanocomposites via absorption & emission matching, Mater. Chem. Phys. 220 (2018) 278–285.
[27] T. Ming, H.J. Chen, R.B. Jiang, Q. Li, J.F. Wang, Plasmon-controlled fluorescence: beyond the intensity enhancement, J. Phys. Chem. Lett. 3 (2012) 191–202.
[28] W. Ge, X.R. Zhang, M. Liu, Z.W. Lei, R.J. Knize, Y.L. Lu, Distance dependence of gold-enhanced upconversion luminescence in $Au/SiO_2/Y_2O_3$:Yb^{3+}, Er^{3+} nanoparticles, Theranostics 3 (2013) 282–288.
[29] Z.J. Wang, W. Gao, R.B. Wang, J. Shao, Q.Y. Han, C. Wang, J. Zhang, T.T. Zhang, J. Dong, H.R. Zheng, Influence of SiO_2 layer on the plasmon quenched upconversion luminescence emission of core-shell $NaYF_4$:Yb,Er@SiO_2@Ag nanocomposites, Mater. Res. Bull. 83 (2016) 515–521.
[30] J. Kang, Y. Li, Y.N. Chen, A.L. Wang, B. Yue, Y.R. Qu, Y.L. Zhao, H.B. Chu, Core–shell $Ag@SiO_2$ nanoparticles of different silica shell thicknesses: preparation and their effects on photoluminescence of lanthanide complexes, Mater. Res. Bull. 71 (2015) 116–121.
[31] N.S. Abadeer, M.R. Brennan, W.L. Wilson, C.J. Murphy, Distance and plasmon wavelength dependent fluorescence of molecules bound to silica-coated gold nanorods, ACS Nano 8 (2014) 8392–8406.
[32] B. Zheng, L. Lin, Z.H. Feng, Z.P. Yu, Z.Z. Wang, S.Y. Xu, Z.Q. Zheng, Plasmon enhanced near-infrared quantum cutting and simulation analysis of β-$NaYF_4$:Tb^{3+}, Yb^{3+} doped with Ag nanoparticles, Opt. Mater. Exp. 7 (2017) 224–230.
[33] X.C. Ye, C. Zheng, J. Chen, Y.Z. Gao, C.B. Murray, Using binary surfactant mixtures to simultaneously improve the dimensional tunability and monodispersity in the seeded growth of gold nanorods, Nano Lett. 13 (2013) 765–771.
[34] W. Feng, C.M. Han, F.Y. Li, Upconversion-nanophosphor-based functional nanocomposites, Adv. Mater. 25 (2013) 5287–5303.
[35] S. Fischer, N.D. Bronstein, J.K. Swabeck, E.M. Chan, A.P. Alivisatos, Precise tuning of surface quenching for luminescence enhancement in core-shell lanthanide-doped nanocrystals, Nano Lett. 16 (2016) 7241–7247.
[36] F.W. Kang, J.J. He, T.Y. Sun, Z.Y. Bao, F. Wang, D.Y. Lei, Plasmonic dual-enhancement and precise color tuning of gold nanorod@SiO_2 coupled core-shell-shell upconversion nanocrystals, Adv. Funct. Mater. 27 (2017) 1701842.
[37] N. Bogdan, F. Vetrone, G.A. Ozin, J.A. Capobianco, Synthesis of ligand-free colloidally stable water dispersible brightly luminescent lanthanide-doped

upconverting nanoparticles, Nano Lett. 11 (2011) 835–840.
[38] Y. Xu, C.F. Guo, L. Luan, X. Ding, Synthesis and characterization of spherical core-shell particles SiO_2@$AgEu(MoO_4)_2$, Appl. Surf. Sci. 256 (2010) 1798–1802.
[39] D. Zhou, X.M. Lin, A.L. Wang, J.J. Li, Y.R. Qu, H.B. Chu, Y.L. Zhao, Fluorescence enhancement of Tb^{3+} complexes by adding silica-coated silver nanoparticles, Sci. China Chem. 58 (2015) 979–985.
[40] L. Zhao, T. Ming, H.J. Chen, Y. Liang, J.F. Wang, Plasmon-induced modulation of the emission spectra of the fluorescent molecules near gold nanorods, Nanoscale 3 (2011) 3849–3859.
[41] D.M. Wu, A. García-Etxarri, A. Salleo, J.A. Dionne, Plasmon-enhanced upconversion, J. Phys. Chem. Lett. 5 (2014) 4020–4031.
[42] Y.L. Wang, N. Mohammadi Estakhri, A. Johnson, H.Y. Li, L.X. Xu, Z. Zhang, A. Alù, Q.Q. Wang, C.K. Shih, Tailoring plasmonic enhanced upconversion in single $NaYF_4$:Yb^{3+}/Er^{3+} nanocrystals, Sci. Rep. 5 (2015) 10196.
[43] Q.Q. Zhan, X. Zhang, Y.X. Zhao, J. Liu, S.L. He, Tens of thousands-fold upconversion luminescence enhancement induced by a single gold nanorod, Laser Photon. Rev. 9 (2015) 479–487.
[44] J. Li, J.H. Zhang, Z.D. Hao, X. Zhang, J.H. Zhao, Y.S. Luo, Intense upconversion luminescence and origin study in Tm^{3+}/Yb^{3+} codoped calcium scandate, Appl. Phys. Lett. 101 (2012) 121905.
[45] S. Karaveli, R. Zia, Spectral tuning by selective enhancement of electric and magnetic dipole emission, Phys. Rev. Lett. 106 (2011) 193004.
[46] V.K. Tikhomirov, L.F. Chibotaru, D. Saurel, P. Gredin, M. Mortier, V.V. Moshchalkov, Er^{3+}-doped nanoparticles for optical detection of magnetic field, Nano Lett. 9 (2009) 721–724.